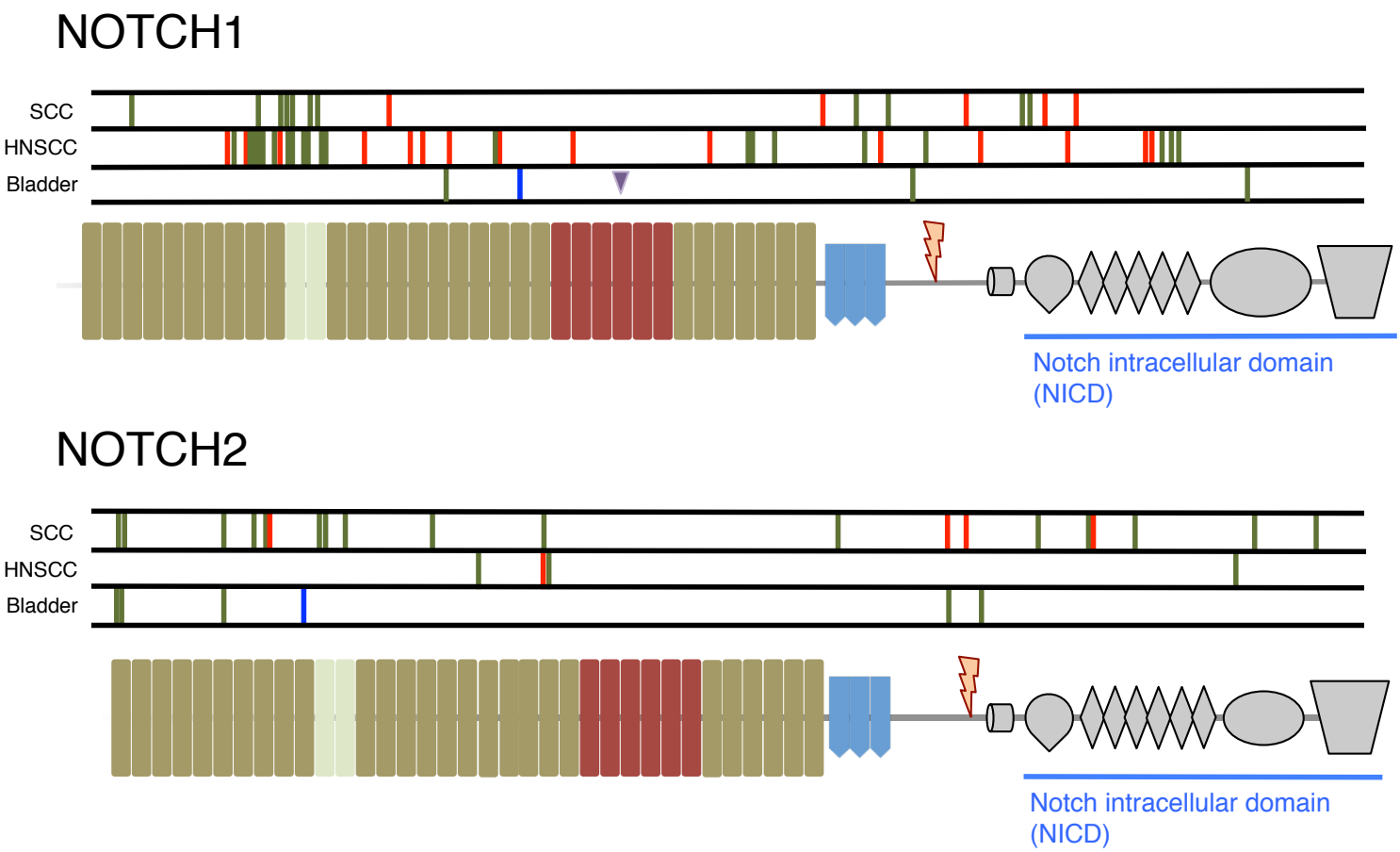

Supplemental Figure 1. Diagram depicting the mutations found in *NOTCH1* and *NOTCH2* receptors. The diagram represents mutations found in both cutaneous and lung SCC squamous cell carcinomas (SCC), head and neck squamous cell carcinomas (HNSCC) and three independent genome wide studies in bladder cancer. Missense mutations are indicated in green; insertions, as arrowheads; nonsense mutations, in red; the mutations functionally analyzed in our work are represented in blue.

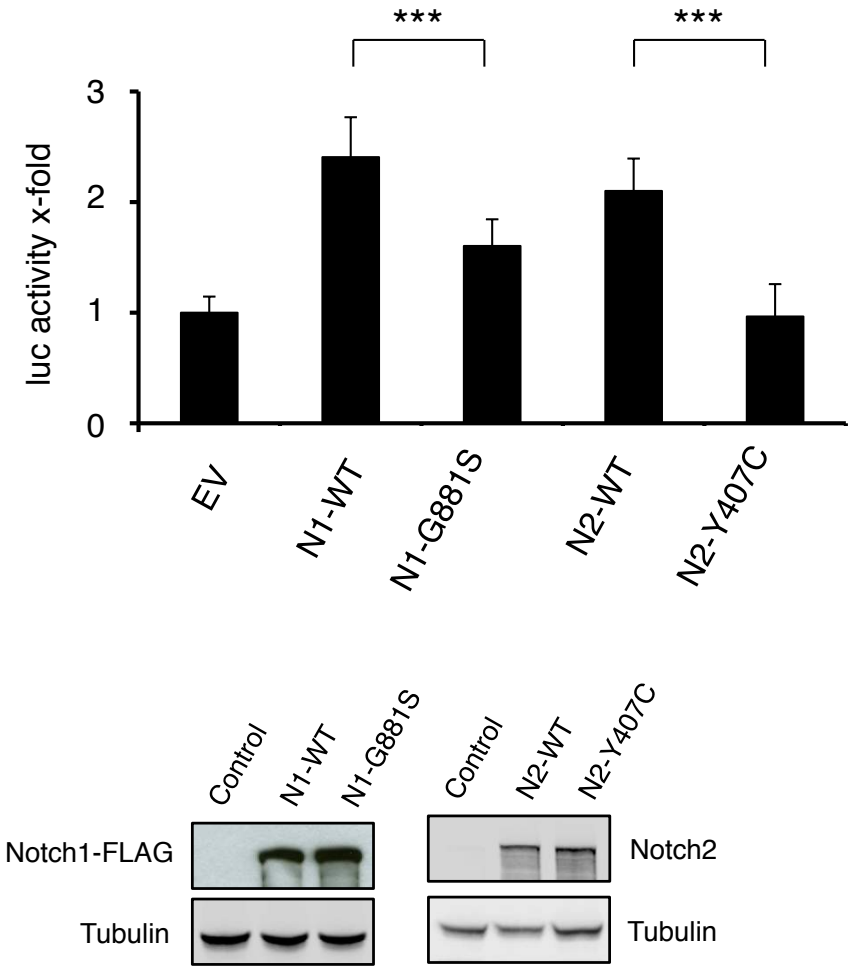

Supplemental Figure 2. The selected missense mutations in NOTCH1 and NOTCH2 cause a decrease in Notch signaling. HEK-293T cells were co-transfected with a luciferase reporter gene under the regulation of an RBPJ-responsive promoter, and with constructs carrying the indicated forms of NOTCH1 (N1) or NOTCH2 (N2). Subsequently, cells overexpressing the Notch ligand JAGGED1 were added in order to activate Notch signaling, and the resulting luciferase activity was measured. Bars represent the average of 5 independent experiments (n=5). Error bars represent standard deviation. Statistical significance was assessed using Student's t test: ***, $p<0.001$. The bottom part shows that the levels of overexpression achieved by transfection were similar in all four cases. NOTCH levels were assessed by immunoblot (tubulin and FLAG immunoblots were performed in two different but equivalent gels).

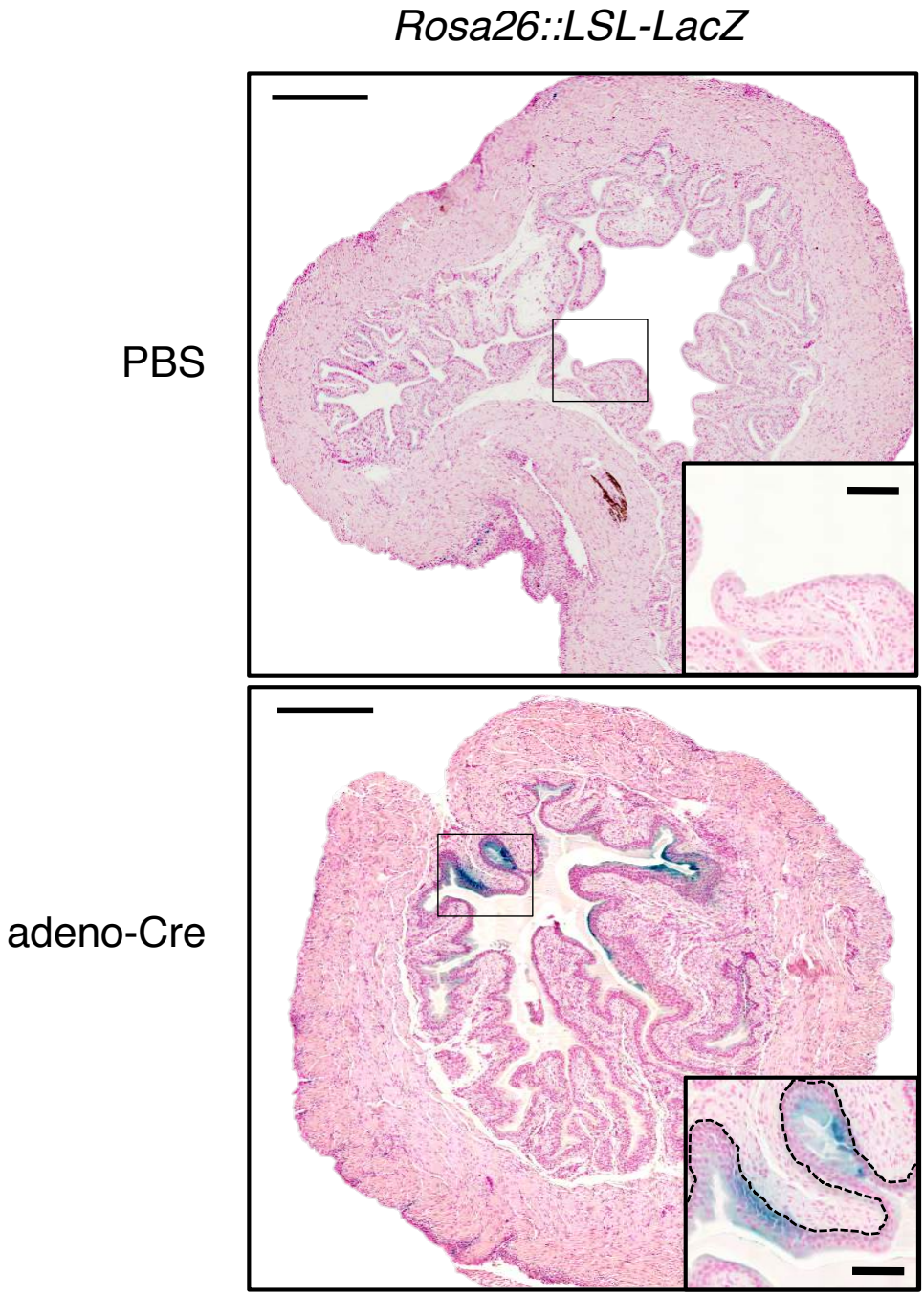

Supplemental Figure 3. Intravesical inoculation of adeno-Cre is effective for excision of *LoxP*-flanked alleles. Bladders from *Rosa26::LSL-LacZ* mice were inoculated intravesically with PBS (upper panel) or adeno-Cre (bottom panel), and stained for LacZ activity. Dashed line in the inserted panel represents the basal layer. Size bars represent 500 μm for the larger panels, and 100 μm for the insets.

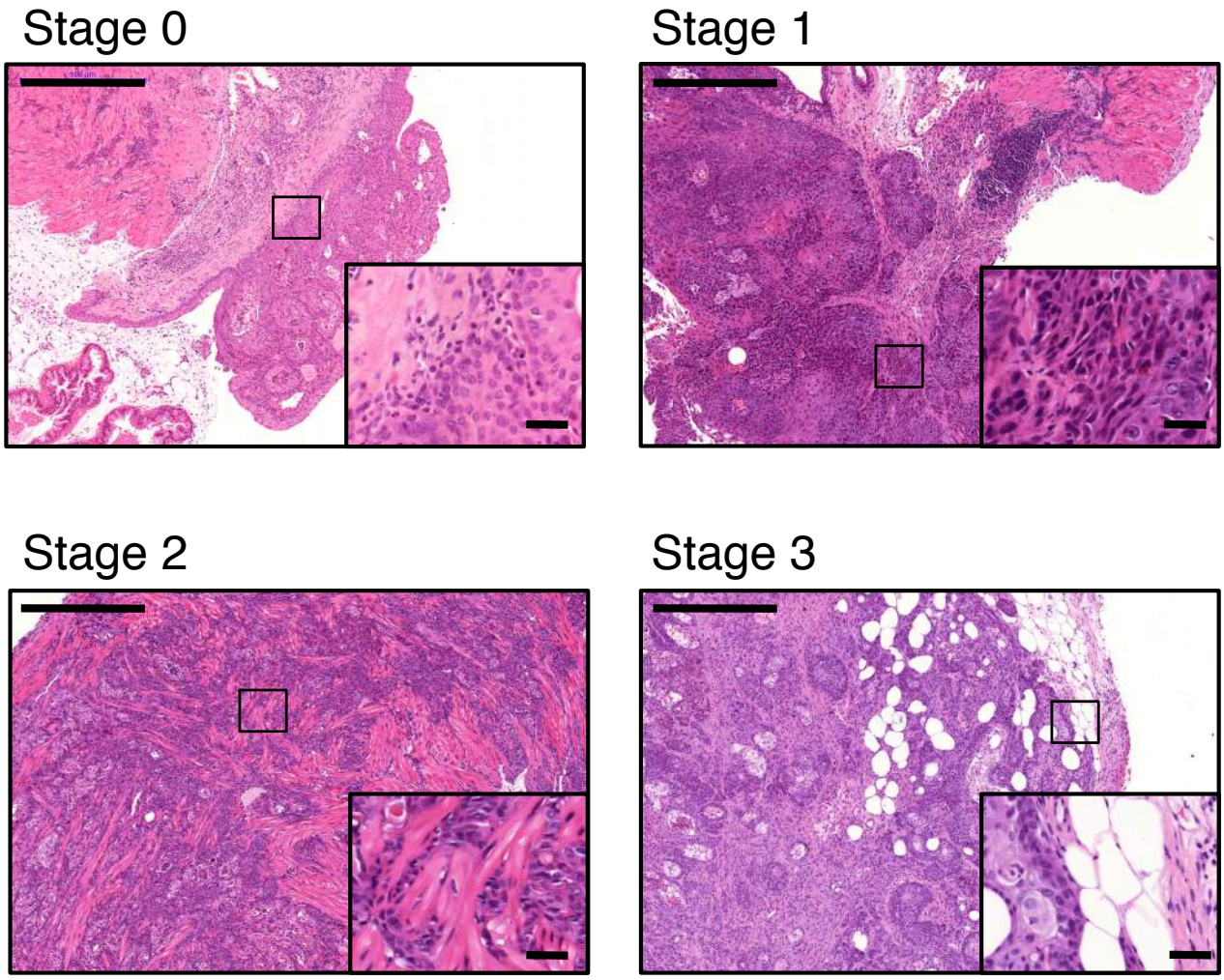

Supplemental Figure 4. Bladder carcinoma stages. Hematoxylin & eosin staining of tumor samples belonging to each of the four different histological groups of mouse bladder carcinomas, namely: non-invasive papillary tumors (stage 0), tumors invading the underlying layer (stage 1), tumors invading the muscular layer (stage 2), and tumors affecting perivesical tissue (stage 3). Scale bars represent 500 μm for the larger panels and 50 μm for the insets.

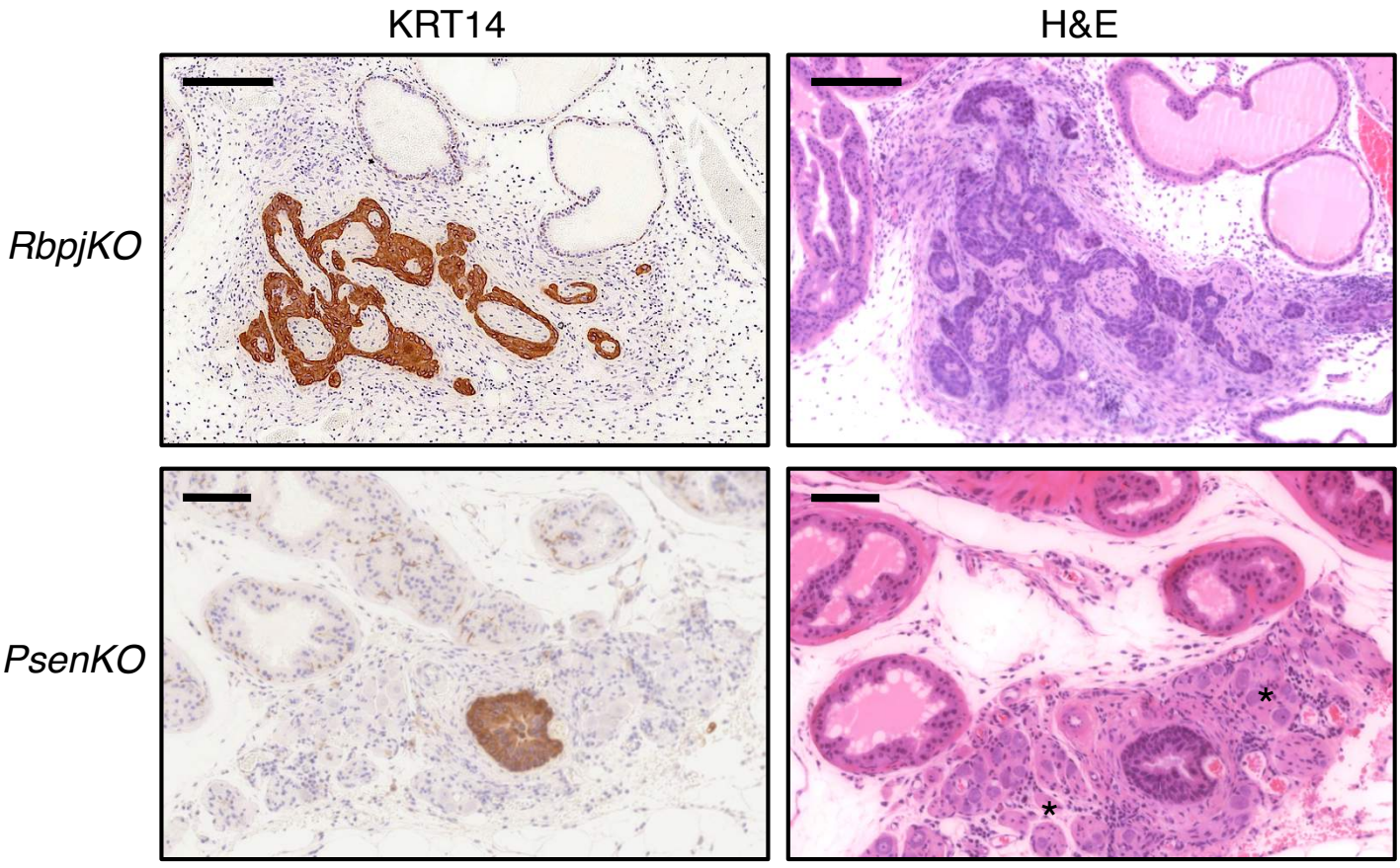

Supplemental Figure 5. Prostate invasion of bladder carcinomas in *PsenKO* and *RbpjKO* mice. Examples of invasion of the prostate stroma by KRT14-positive cells in mice of the indicated genotypes. The example chosen for *PsenKO* prostate invasion presents KRT14-positive cells surrounding a neuronal ganglion (stars), thus indicating perineural invasion. Scale bars represent 200 μm for the top panels, and 100 μm for the bottom panels

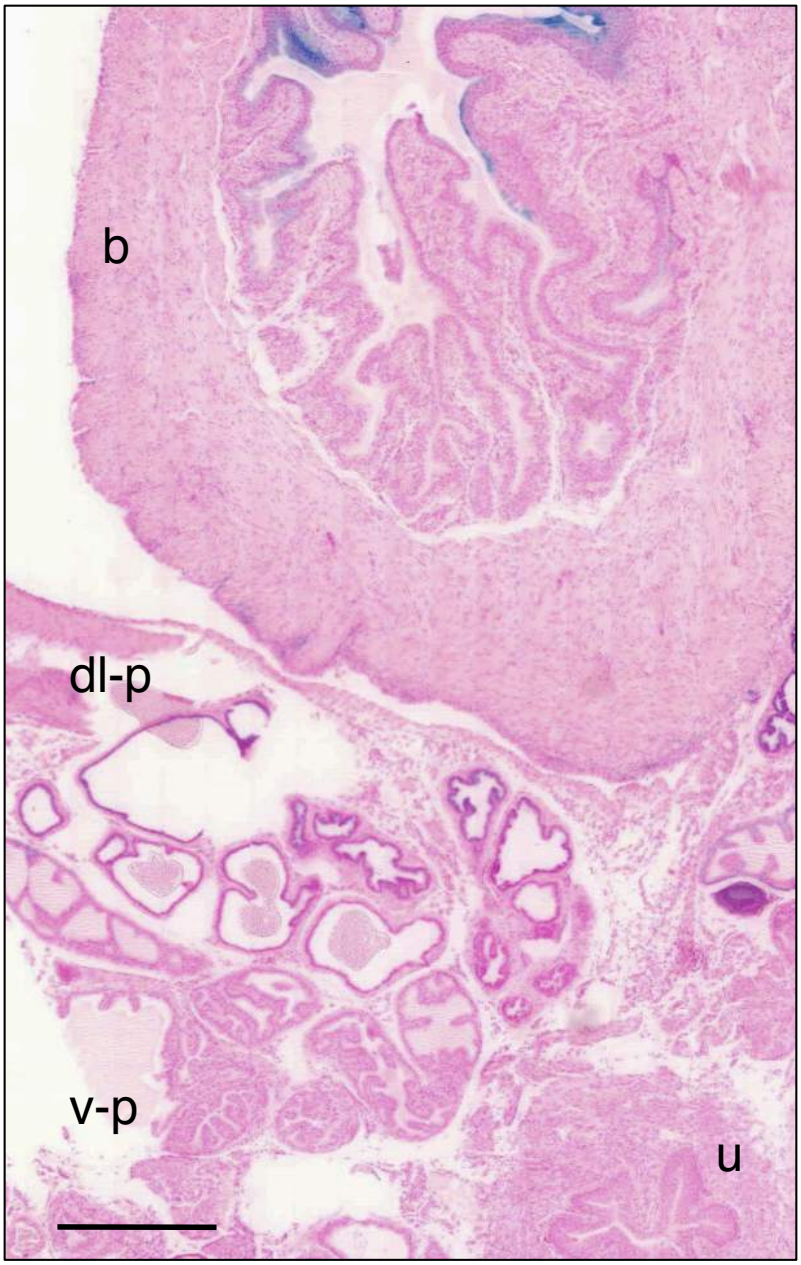

Supplemental Figure 6: Intravesical adeno-Cre virus inoculation infects the urinary bladder but not the nearby tissues. Representative photograph of the bladder and nearby tissues of the same *Rosa26::LSL-LacZ* mouse shown in Supplemental Figure 3. Abbreviations: b, bladder; v-p, ventral prostate; dl-p, dorsolateral prostate, u, urethra. Size bar = 500 μm.

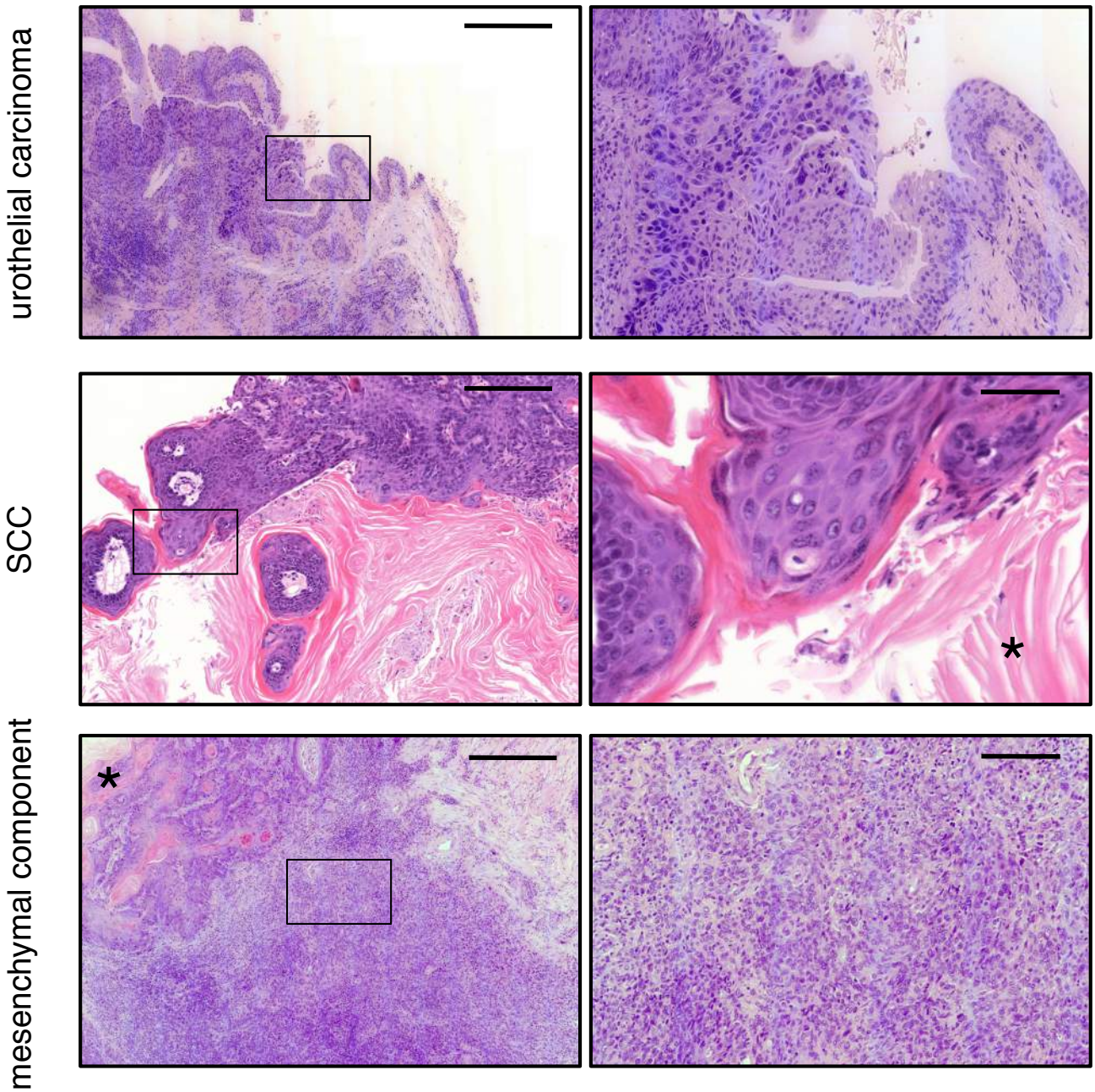

Supplemental Figure 7. Histological examples. Top, representative example of a urothelial carcinoma. These carcinomas are characterized by increased thickness, loss of cell polarity, enlarged nuclei and mild pleomorphism. Middle, representative example of a bladder squamous cell carcinoma (SCC). These carcinomas are characterized by sheets of polygonal, well-differentiated epithelial cells, with variable degrees of atypias and evident production of keratin (asterisks). Bottom, example of a region undergoing EMT near an SCC (marked by the asterisk). Scale bars represent 200 μm for the left panels and 50 μm for the right panels (insets).

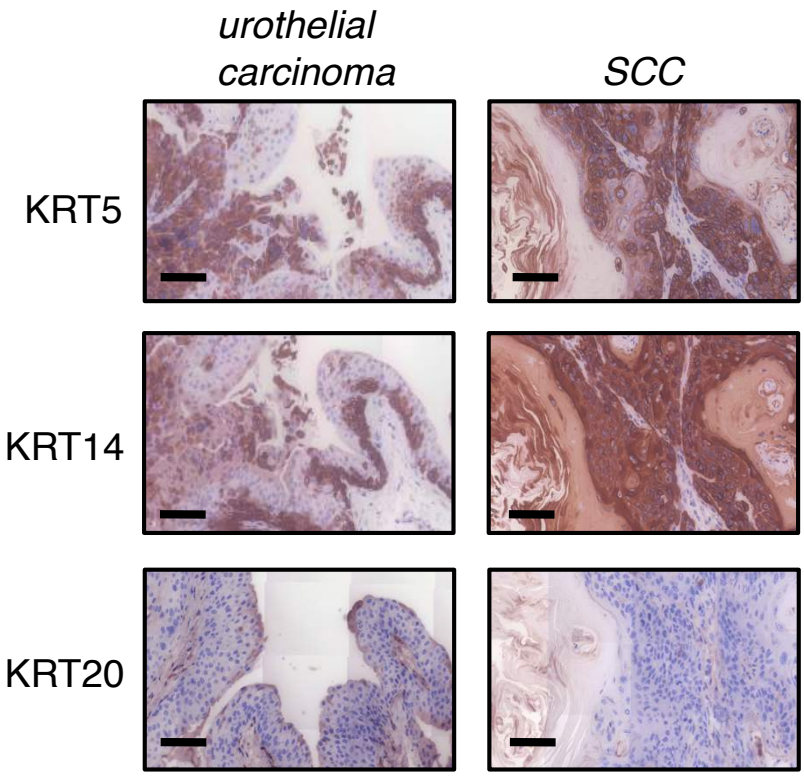

Supplemental Figure 8: Molecular features of SCCs. Representative examples of the pattern of cytokeratin expression in urothelial carinomas (left column) and in squamous cell carcinomas (right column). Urothelial carcinomas restrict KRT5 and KRT14 expression to the basal layer, and KRT20 to the suprabasal layer. In contrast, SCCs express the basal markers KRT5 and KRT14 in all the tumoral cells, and lose the suprabasal marker KRT20. Size bar = 50 μm.

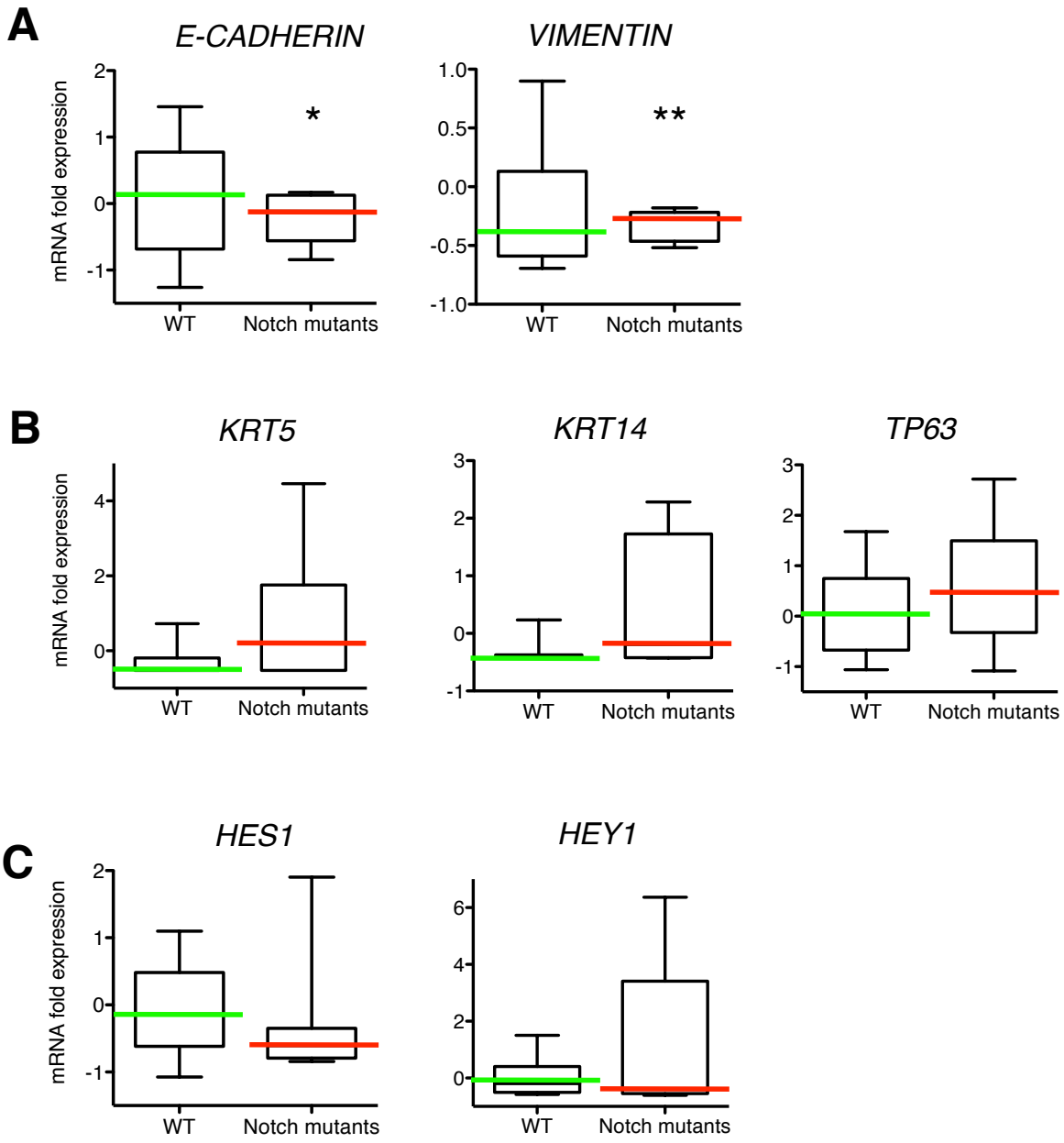

Supplemental Figure 9. Human bladder carcinomas harboring missense mutations in NOTCH1 and NOTCH2 present EMT (A) and squamous features (B) and lower levels of Notch target genes (C). RNAseq data from TCGA was analyzed for the indicated genes, and grouped into WT and Notch missense mutants, as indicated. Statistical significance was assessed using the Student's t test: *, $p<0.05$; **, $p<0.01$.

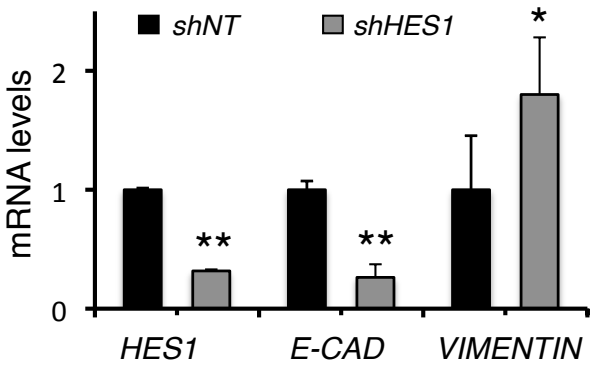

Supplemental Figure 10. HES1 inhibition induces EMT. Levels of mRNA of the indicated genes were determined in T24 cells infected with *shHES1* or with *shNT*. Error bars correspond to S.E.M. of at least three replicates. Statistical significance was assessed by Student's t test: *, $p<0.05$; **, $p<0.01$.

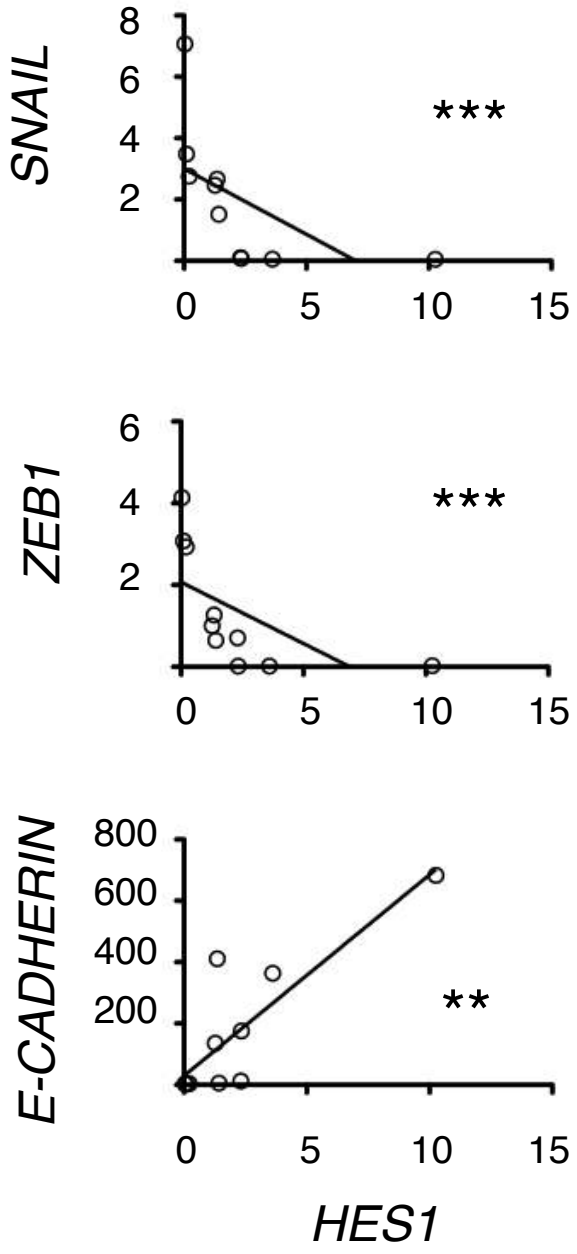

Supplemental Figure 11. Validation of the cDNA array data by qRT-PCR. A subset of the RNA samples used for Figure 6A were analyzed for the indicated genes by qRT-PCR. Graphs represent linear correlations with *HES1* mRNA. Values are relative to reference gene. RNA from 10 different tumors was used for these analysis. Statistical significance was assessed using Spearman test: **, $p<0.05$; ***, $p<0.01$

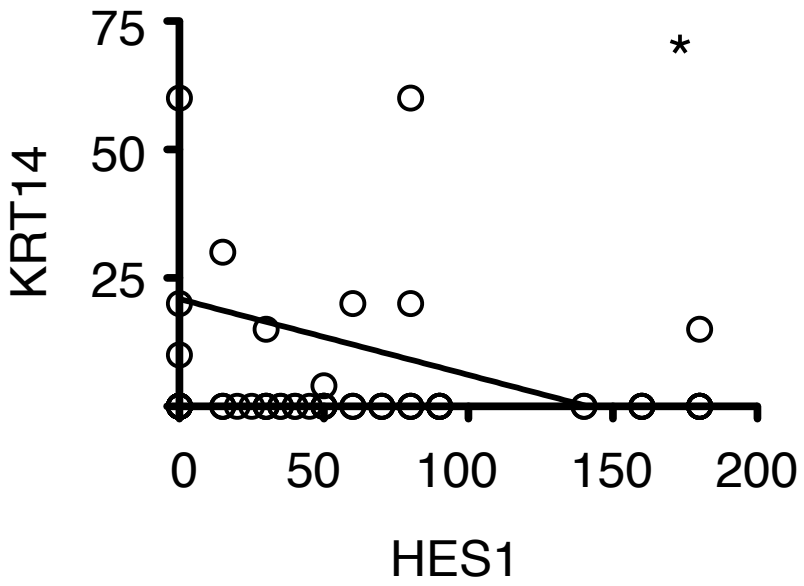

Supplemental Figure 12. KRT14 expression inversely correlates with HES1 levels in human bladder tumors. A subset of tumor samples from the same set than Figure 6C were analyzed for KRT14 expression by IHC. The graph represents the correlation for the histoscores of HES1 (as in Figure 6C) and KRT14. A total of 74 tumor samples were used for this analysis. Statistical significance was assessed using Spearman test: *, $p<0.05$.

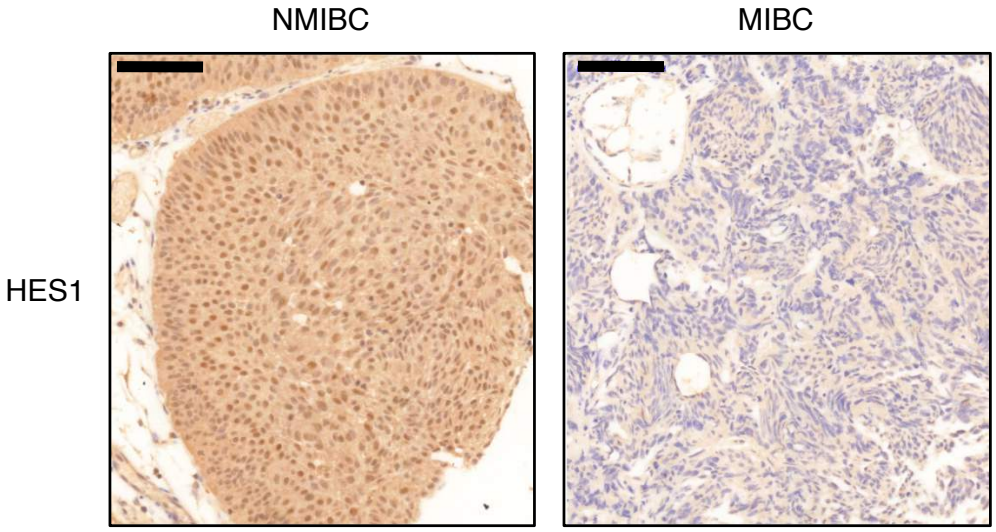

Supplemental Figure 13. HES1 levels in human bladder carcinomas. Representative examples of the HES1 stainings used for the determination of the HES1 histoscore used in Figure 6C. Size bars represent 100 μm.

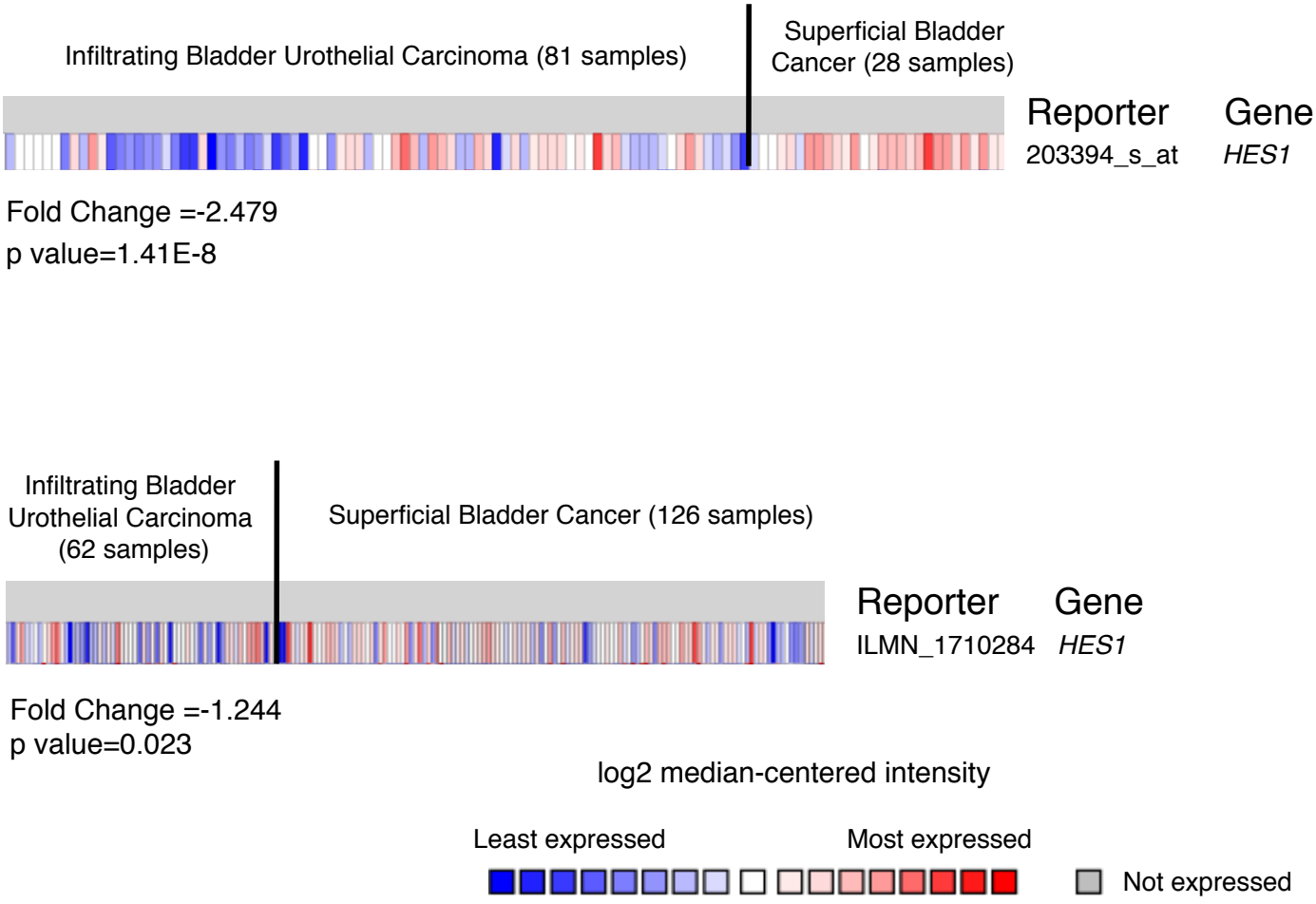

Supplemental Figure 14. *HES1* gene expression is decreased in infiltrating human bladder tumors. Heat maps generated at Oncomine (http://www.oncomine.org) (33) by analyzing data deposited in Oncomine from two original studies, top (34) and bottom (35). Levels of upregulation and downregulation of *HES1* transcript in each sample are indicated by gradients of red and blue, respectively. Each vertical bar represents a single sample. The number of independent clinical samples analyzed of each tumor subtype is provided. The fold change (in log2) and corresponding p value of the variations in the infiltrating vs superficial tumors is shown for each dataset.

SUPPLEMENTAL METHODS

Notch pathway inactivation promotes bladder cancer progression

Antonio Maraver, Pablo J. Fernandez-Marcos, Timothy P. Cash, Marinela Mendez, Marta Dueñas, Paolo Maietta, Paola Martinelli, Maribel Muñoz-Martin, Mónica Martínez-Fernández, Marta Cañamero, Giovanna Roncador, Jorge L. Martinez-Torrecuadrada, Dimitrios Grivas, Jose Luis de la Pompa, Alfonso Valencia, Jesús M. Paramio, Francisco X. Real, Manuel Serrano

Mutagenesis

Plasmids carrying the full-length cDNA of human *NOTCH1* (pcDNA3-NOTCH1) and *NOTCH2* (pcDNA3-NOTCH2) under cytomegalovirus promoter were kind gifts from Adolfo Ferrando and Anna Bigas, respectively. We performed mutagenesis in *NOTCH1* and *NOTCH2* genes using the QuikChange II XL Site-Directed Mutagenesis Kit (Agilent technologies), that provide high fidelity for large plasmids, following manufacturer instructions. The obtained colonies were analyzed by DNA sequencing to confirm the mutation.

Primers used for the mutagenesis:

 # N1G881S

Forward-5'-CTG AGC CCG TGC CGG CAC GAC GCA TCC TGC CAG AAC ACC-3'

Reverse-5'-GGT GTT CTG GCA GGA TGC GTC GTG CCG GCA CGG GCT CAG-3'

 # N2Y407C

Forward-5'-GCA CCT GCC CAC AAG GCT GCA AAG GGG CTG ACT GCA C-3'

Reverse-5'-GTG CAG TCA GCC CCT TTG CAG CCT TGT GGG CAG GTG C-3'

Primers used for sequencing:

 # N1G881S

Forward-5'-AGC TTC TCC TGT GTC TGC-3'

Reverse-5'-TGG CAC ACT CGT TGA TGT-3'

 # N2Y407C

Forward-5'-GGG CAC TGT GTG ACA CCA AC-3'

Reverse-5'-GAC CTC GTT GTG AGA TGG-3'

Luciferase assays

Luciferase assays were done in T24 and HEK293 cells using FuGENE® 6 (Promega) for the transfections. An adapted protocol from the described before by José Luis de la Pompa that kindly provided us with the luciferase based Notch reporter pGL3basic-10xCBF1-Luc (52) was followed. We transfected cells with NOTCH1 or NOTCH2 full length *wt* or mutated as described above together with the Notch signaling reporter pGL3basic-10xCBF1-Luc (53) and *Renilla* luciferase to normalize the data. 18 h post-transfection, cells were co-cultured with HEK293 cells stably expressing the Notch ligand JAG1 (54). Luminescence was measured 48 hours later using a Glomax luminometer (Promega).

Mutation modeling

The mutation Y407C falls in the EGF-like 10 domain (Pfam (55) ID PF00008) of NOTCH2. The main structure of EGF-like domains is a two-stranded β-sheet followed by a loop to a short C-terminal, stabilized by 3 disulfide bridges (56). In order to evaluate the possible impact of the insertion of a new cysteine on the native ones, we used a disulfide predictor. We used different algorithms and we assessed the prediction using the UniProt (57) annotation for NOTCH2 human (accession ID: Q04721). The best method was DIpro (58), that was able to reconstruct the native disulfide bridges annotated in Uniprot for domains 9-10-11 (see table below). We used 3 consecutive domains in order to test the precision of the methods. After that we predicted the disulfide bridge pairs for the mutated sequence 9-10(Y407C)-11-12.

Domain	UniProt	DIpro (wild type)	DIpro (Y407C mutation)
9	342-352	342-352	342-352
	347-362	347-362	347-362
	364-373	364-373	364-373
10	379-390	379-390	379-390
	384-401	384-401	384-401
	403-412	403-412	407-412

11	419-433	419-433	419-433
	427-442	427-442	427-442
	444-453	444-453	444-453

In order to test the structural change derived from this non-native disulfide bridge and since there is no structure available of the EGF domain 10, we generated models of the 3 domains 9-10-11, one of the wild type and another of the mutated protein. First we searched for a template using HHpred (59), a state of art method for the template-based structure prediction (60), and we found as best template the protein with PDB (61) accession 4d90 (Developmental endothelial cell locus-1) and the protein with PDB accession 2vj3 (human NOTCH1 EGFs domains 11-13). We selected the second one because the structure (15) represents the binding site of Jagged/Serrate DSL domain of NOTCH1, a close homologue of NOTCH2 and the alignment presents a ~40% identity between the two sequences with a limited number of gaps. After the modification of the alignment in order to correct wrong pairing of a cysteine we run the MODELLER (58) program and we obtained the wild type model. For the generation of the mutated model, we used the same alignment, except for the change of the Tyr 407 into Cys. In this run we provided to the program the new pairing of the cysteines in the structure. The model obtained has been used as starting structure for the simulations.

Simulations were performed with the GROMACS4 MD code, using the Amber99SB-ILDN (62) all-atom force field and the TIP3P water model. The equations of motion were integrated with a time step of 0.2 fs. All covalent bonds were constrained to their equilibrium values using the LINCS algorithm. The electrostatic interactions were calculated by the Particle Mesh Ewald algorithm, and a cut-off of 0.9 nm was used both for Lennard–Jones and for the real-space Coulomb interactions. After being solvated, the system have been minimized and heated step by step from 0 K to 300 K constraining the heavy atoms with a decreasing force constant. All the simulations were performed using a cubic box with periodic boundary conditions. The systems were equilibrated for 1 ns in the isobaric–isothermal ensemble (T=300 K,P=1 atm) controlled by the Nose-Hoover thermostat and the isotropic Parrinello–Rahman barostat, resulting in an average volume of 125.7 nm^3. The final production runs were 1 ns long.

Mice

Psen1$^{f/f}$;*Psen2*$^{-/-}$ mice (18) and *Rbpj*$^{f/f}$ have been already reported (19). Recombination of *loxP* sites was performed by injection of adeno-Cre commercially produced at the University of Iowa, into the urinary bladder as previously described (20).

Monoclonal antibody generation

The GST-His-MsHes-1 fusion protein was expressed in *Escherichia coli* strain BL21 (DE3), purified by affinity chromatography on a GSTrap™ column (GE Healthcare, Little Chalfont, UK) and used as immunogen. Two Wistar rats were injected intraperitoneally (three times at 14-day intervals) with 100 μg of His-Hes-1 fusion protein and Freund's complete adjuvant (Difco, USA). A 150-μg booster of the recombinant Hes-1 protein was injected intraperitoneally, and fused three days later, as described previously (63). Hybridoma supernatants were screened by ELISA and in HEK293T-Hes-1 transfected cells. The rat mAb that was raised against Hes-1 (clone HS395A) was cloned by the limiting dilution technique.

Histopathology and immunohistochemistry in mice

Tissues were dissected, fixed in 10%-buffered formalin (Sigma) and embedded in paraffin. Sections 5 μm-thick were stained with hematoxylin and eosin (H&E) or were subjected to antigen retrieval. Antibodies used for immunohistochemistry were mouse monoclonal to KRT5 (D5/16 B4 from DAKO), mouse polyclonal to KRT14 (PRB-115P from Covance), mouse monoclonal to KRT20 (Ks20.8 from DAKO), rat monoclonal to HES1 (HS395A/A7, CNIO), rabbit monoclonal to VIMENTIN (D21H3, Cell Signaling), and mouse monoclonal to E-CADHERIN (NCH-38 from DAKO). Histopathological grading was performed in a semiquantitative way by our expert pathologist (M.C.). In the case of KERATINS and HES1, both intensity of staining and percentage of stained cells were scored from 0 to 3. In the case of E-CADHERIN, the presence of zones with loss of expression was scored as 0, while a homogeneous expression was scored as 1.

Histopathology and immunohistochemistry in humans

We used two sets of human tumor samples. A set of tumors from patients evaluated at the Urology Department of the University Hospital “12 de Octubre” between October 2009 and March 2011, and diagnosed with a T1 G3 or T2 bladder cancer (32). From this set of samples we analyzed RNA samples. A second set of tumor samples was obtained from the EPICURO

consortium and these samples were used for histology and immunohistochemistry. Staging and grading were performed as described (64). Expert pathologists reviewed diagnostic slides from all tumor blocks. We categorized TaG1 and TaG2 tumors as low-risk NMIBC; TaG3, T1G2 and T1G3 tumors were categorized as high-risk NMIBC; and ≥T2 tumors were categorized as MIBC.

HES1 and KRT14 expression (using the rabbit polyclonal sc-25392, Santa Cruz Biotechnology and mouse polyclonal PRB-115P from Covance) from tissue microarrays containing tumors from the Epicuro consortium (add ref EPICURO) (51). Stained samples were scored based on the intensity of expression (0-3) and the proportion of reactive cells (0-100%); histoscore was determined by multiplying both parameters, expressed as a range from 0-300. When more than one core was available from a given tumor, the mean score was used.

Cell culture

T24 human bladder carcinoma and HEK-293T human embryonic kidney cells were purchased at ATCC. The siGENOME SMARTpool HES1 siRNA was obtained from Thermo Scientific Dharmacon RNAi Technologies (M-007770-01) and transfected into T24 cells following manufacturer instructions. As control we used the siGENOME Non-Targeting siRNA #1, (D-001210-01) also from Thermo Scientific Dharmacon. pLKO.1 vector encoding for an shRNA against HES1 or a Non Targeting shRNA were kindly donated by Dr Anna Bigas (26). T24 cells were infected with the corresponding lentiviruses and selected for 3 days with puromycin. For luciferase assays, 293T cells were transfected with Fugene 6 (Promega), and T24 cells with Lipofectamine LTX (Invitrogen), and 48 later luciferase activity or full length of Notch proteins overexpression were assessed. For HA-HES1 overexpression we used the pMSCV-HA-HES1 kindly donated by Dr. Adolfo Ferrando's laboratory (31) or an empty pMSCV. T24 cells were infected with the produced retroviruses and selected for 3 days with puromycin before proceeding to the ChIP protocol.

Immunofluorescence

Paraffin sections were deparaffinized and subjected to a Tris/EDTA treatment for antigen retrieval, permeabilized with PBS-0.5% Triton X-100 for 30' and blocked with Blocking reagent (Roche) in blocking solution (0.1M Tris-HCl, 0.15M NaCl, 0.5% Blocking Reagent) for 30'. After rinsing in PBS, samples were incubated with the following primary antibodies: E-CADHERIN (mouse NCH-38, DAKO, 1:200); VIMENTIN (chicken AB5733, Millipore, 1:200) and HES1 (rat 395A/A7, CNIO, 1:50), for 1h at 37ºC. After washing 3 times with PBS,

secondary antibodies were added at 1:200 dilution for 45' at RT. After washing, slides were incubated in a 100 μg/ml DAPI solution in PBS for 5', and mounted.

Chromatin immunoprecipitation

Cells were crosslinked with 1% formaldehyde for 15 min at room temperature. Crosslinking was stopped by the addition of glycine to a final concentration of 0.125 M. Fixed cells were lysed in lysis buffer (1% SDS, 10 mM EDTA, 50 mM Tris-HCl, pH 8.0) and sonicated for 60' using a Covaris sonicator. An aliquot of 60 μg was reserved as input. For immunoprecipitation, 5mg of protein were diluted in dilution buffer (1% Triton X-100, 2 mM EDTA, 150 mM NaCl and 20mM Tris-HCl, pH 8.0, containing protease inhibitors), and precleared with 60 μl of A/G plus-agarose (Santa Cruz Biotechnology). The antibodies used for the O/N immunoprecipitation at 4ºC were: Rabbit HA ab9110 (Abcam) and Rabbit non-targeting IgG (Jackson Immuno Research). Immune complexes were precipitated with A/G plus-agarose and washed sequentially with low-salt immune complex wash buffer (0.1% SDS, 1% Triton X-100, 2 mM EDTA, 20 mM Tris-HCl, pH 8.1, 150 mM NaCl), high-salt immune complex wash buffer (0.1% SDS, 1% Triton X-100, 2 mM EDTA, 20 mM Tris-HCl, pH 8.1, 500 mM NaCl), LiCl immune complex wash buffer (0.25 M LiCl, 1% NP-40, 1% deoxycholate-Na, 1 mM EDTA, 10 mM Tris-HCl, pH 8.1), and TE buffer, and then eluted in elution buffer (1% SDS, 0.1 M NaHCO3). All samples, including inputs, were de-crosslinked, treated with proteinase K, and DNA was extracted with phenol–chloroform and resuspended in 0.5xTE buffer.

HES1 binds two similar sequence motifs, known as class C sites and N-boxes. We searched for these sites in the upstream 5000bp from the translation starting site of the following human gene promoters: SNAIL, SLUG, ZEB1, ZEB2, VIMENTIN and TWIST, and designed primers targeting one or two regions of high density of putative HES1 binding sites, as described elsewhere (27). The primers used for detection of binding to the different genes were as follows:

#*SNAIL* site 1:	Forward: 5'-GGT GTG GGG TGC TTA TAG GT-3'
	Reverse: 5'-GGG GTG GCT CTG AAA TAA ACC-3'
#*SNAIL* site 2:	Forward: 5'-CAT TTC AAG CCG CCG AGA G-3'
	Reverse: 5'-GTG GCA TTG ACG AGG GAA AC-3'
#*SNAIL2* site 1:	Forward: 5'-ACC TCA CCC TCC AAA CAC AC-3'
	Reverse: 5'-CAG TGG TGA TGT CAA GAC TTG T-3'

#ZEB1 site 1:	Forward: 5'-CCA TTG CCC TCC TTT GTT CC-3'
	Reverse: 5'-TCC CAT AAA GCC GCT ACT CA-3'
#ZEB1 site 2:	Forward: 5'-TCA AAT TCA GCA GTG CCC AC-3'
	Reverse: 5'-GGC TTT ACG ACA TCA CCT TCC-3'
#ZEB2 site 1:	Forward: 5'-CGT TTG CGG AGA CTT CAA GG-3'
	Reverse: 5'-GGG ATA ATT GAA GCG CCC TG-3'
#ZEB2 site 2:	Forward: 5'-CCC TCT CAG CAA ATG TGT GG-3'
	Reverse: 5'-TAA CCC TTT CTC TGC CGG G-3'
#VIMENTIN site 1:	Forward: 5'-GGG GAA CAG TGG AAA ATG AGG-3'
	Reverse: 5'-CTG CAG AGG AGG TTG AGG A-3'
#VIMENTIN site 2:	Forward: 5'-CAG GAC TCG GTG GAC TTC TC-3'
	Reverse: 5'-CTT GTC GAT GTA GTT GGC GA-3'
#TWIST site 1:	Forward: 5'-TCG GAC AAG CTG AGC AAG AT-3'
	Reverse: 5'-CTC GTC GCT CTG GAG GAC-3'

RNA analysis and qRT-PCR

For patient tissue, total RNA was isolated using miRNeasy Mini Kit (Qiagen) according to the manufacturer's instructions and DNA was eliminated (Rnase-Free Dnase Set Qiagen). Reverse transcription was performed using the Omniscript RT Kit (Qiagen) and a primer mix specific for all genes of interest using 10ng of total RNA. PCR was performed in a 7500 Fast Real Time PCR System using Go Taq PCR master mix (Promega) and 1 µl of cDNA as a template. Melting curves were performed to verify specificity and absence of primer dimerization. Reaction efficiency was calculated for each primer combination, and *TBP* gene was used as reference gene for normalization (65). For T24 cells, total RNA was extracted with Trizol (Life Technologies) and for generation of cDNA we used Ready-to-Go (GE Healthcare). Quantitative real-time PCR was performed using an ABI PRISM 7700 (Applied Biosystems), using DNA Master SYBR Green I mix (Applied Biosystems) and *β-ACTIN* was used as reference gene for normalization.

Primers used were:

# HES1	HES1-F:	5'-AAG AAA GAT AGC TCG CGG CAT-3'
	HES1-R:	5'-CCA GCA CAC TTG GGT CTG T-3'
# E-CADHERIN	E-CADHERIN-F:	5'-CGA GAG CTA CAC GTT CAC GG-3'
	E-CADHERIN-R:	5'-GTG TCG AGG GAA AAA TAG GCT G-3'

# VIMENTIN	VIMENTIN-F:	5'-AGT CCA CTG AGT ACC GGA GAC-3'
	VIMENTIN-R:	5'-GGT TCC TTT AAG GGC ATC CAC-3'
# SNAIL	SNAIL-F:	5'-CGA GCT GCA GGA CTC TAA T-3'
	SNAIL-R:	5'-CCA CTG TCC TCA TCT GAC A-3'
# SLUG	SLUG-F:	5'-TTC GGA CCC ACA CAT TAC CT-3'
	SLUG-R:	5'-TTG GAG CAG TTT TTG CAC TG-3'
# ZEB1	ZEB1-F:	5'-GAT GAT GAA TGC GAG TCA GAT GC-3'
	ZEB1-R:	5'-ACAGCAGTGTCTTGTTGTTGT-3'
# ZEB2	ZEB2-F:	5'-CAA GAG GCG CAA ACA AGC C-3'
	ZEB2-R:	5'-GGT TGG CAA TAC CGT CAT CC-3'
# β-ACTIN	ACT-F:	5'-CAA GGC CAA CCG CGA GAA GAT-3'
	ACT-R:	5'-CCA GAG GCG TAC AGG GAT AGC AC-3'
# TBP	TBP-F:	5'-CAA GGC CAA CCG CGA GAA GAT-3'
	TBP-R:	5'-CCA GAG GCG TAC AGG GAT AGC AC-3'

The difference in PCR cycles with respect to *β-ACTIN* or *TBP* (ΔCt) for a given experimental sample was subtracted from the corresponding ΔCt of the reference sample (such as wild-type) (ΔΔCt). Values of ΔΔCt were converted into fold expression ($2^{\Delta\Delta Ct}$).

Invasion assays

Invasion assays were performed using BD BioCoat™ Matrigel™ Invasion Chamber according to the manufacturer's instructions (VWR International, Catalog # 354480). T24 cells were trypsinized, counted and washed in serum free medium. $1x10^5$ cells in 500 µl serum-free medium were plated in the previously rehydrated chamber. 500µl of 10% FBS DMEN medium were used as chemo-attractant (bottom-surface). After 20h incubation in a humidified tissue culture incubator at 37ºC and 5% CO2 atmosphere, cells were fixed with 4% PFA for 15 minutes at room temperature. Nuclei were stained with DAPI and visualized by confocal microscopy. Images were acquired in a Leica TCS-SP5 (AOBS) and quantified with IMARIS software v5.0 (Bitplane) by counting cells on both sides of the matrigel filter. 6 Photographs were taken by chamber and each condition was done in triplicate. Percentages were calculated considering the number of cells that invaded the matrigel filter compared to the total number of cells in both sides of the chamber.

Microarray analysis

RNA was purified as commented above and analyzed by Bioanalyzer electropherogram. Samples showing RNA integrity number (RIN) above 8 were selected for microarray analysis. Genome-wide transcriptome experiments were performed using the Affymetrix HuGene-1_0-st-v1 microarray at the Genomics Facility of the Cancer Research Center (Salamanca, Spain) using standard procedures. Datasets have been deposited in GEO (GSE38264). The other 2 analysis described in Supplementary Figure 10 has been performed using available data sets previously described (33-35).

REFERENCES

52. Luxan G, Casanova JC, Martinez-Poveda B, Prados B, D'Amato G, MacGrogan D, Gonzalez-Rajal A, Dobarro D, Torroja C, Martinez F, et al. Mutations in the NOTCH pathway regulator MIB1 cause left ventricular noncompaction cardiomyopathy. *Nat Med*. 2013;19(2):193-201.

53. McKenzie GJ, Stevenson P, Ward G, Papadia S, Bading H, Chawla S, Privalsky M, and Hardingham GE. Nuclear Ca2+ and CaM kinase IV specify hormonal- and Notch-responsiveness. *J Neurochem*. 2005;93(1):171-185.

54. Chapman G, Liu L, Sahlgren C, Dahlqvist C, and Lendahl U. High levels of Notch signaling down-regulate Numb and Numblike. *J Cell Biol*. 2006;175(4):535-540.

55. Punta M, Coggill PC, Eberhardt RY, Mistry J, Tate J, Boursnell C, Pang N, Forslund K, Ceric G, Clements J, et al. The Pfam protein families database. *Nucleic Acids Res*. 2012;40(Database issue):D290-301.

56. Appella E, Weber IT, and Blasi F. Structure and function of epidermal growth factor-like regions in proteins. *FEBS Lett*. 1988;231(1):1-4.

57. Activities at the Universal Protein Resource (UniProt). *Nucleic Acids Res*. 2014;42(Database issue):D191-198.

58. Cheng J, Saigo H, and Baldi P. Large-scale prediction of disulphide bridges using kernel methods, two-dimensional recursive neural networks, and weighted graph matching. *Proteins*. 2006;62(3):617-629.

59. Soding J, Biegert A, and Lupas AN. The HHpred interactive server for protein homology detection and structure prediction. *Nucleic Acids Res*. 2005;33(Web Server issue):W244-248.

60. Mariani V, Kiefer F, Schmidt T, Haas J, and Schwede T. Assessment of template based protein structure predictions in CASP9. *Proteins*. 2011;79 Suppl 10(37-58.

61. Berman HM, Westbrook J, Feng Z, Gilliland G, Bhat TN, Weissig H, Shindyalov IN, and Bourne PE. The Protein Data Bank. *Nucleic Acids Res*. 2000;28(1):235-242.

62. Lindorff-Larsen K, Piana S, Palmo K, Maragakis P, Klepeis JL, Dror RO, and Shaw DE. Improved side-chain torsion potentials for the Amber ff99SB protein force field. *Proteins*. 2010;78(8):1950-1958.

63. Mason DY, Cordell JL, and Pulford KAF. *Production of monoclonal antibodies for immunocytochemical use*. Bullock, GR, and Petrusz, P, eds. London: Academic Press; 1983.

64. Amaral AF, Mendez-Pertuz M, Munoz A, Silverman DT, Allory Y, Kogevinas M, Lloreta J, Rothman N, Carrato A, Rivas del Fresno M, et al. Plasma 25-hydroxyvitamin D(3) and bladder cancer risk according to tumor stage and FGFR3 status: a mechanism-based epidemiological study. *J Natl Cancer Inst*. 2012;104(24):1897-1904.

65. Bornachea O, Santos M, Martinez-Cruz AB, Garcia-Escudero R, Duenas M, Costa C, Segrelles C, Lorz C, Buitrago A, Saiz-Ladera C, et al. EMT and induction of miR-21 mediate metastasis development in Trp53-deficient tumours. *Sci Rep*. 2012;2(434.